Shear, Strain, and Richardson Number Variations in the Thermocline. Part I: Statistical Description

ROBERT PINKEL

Marine Physical Laboratory, Scripps Institution of Oceanography, La Jolla, California

STEVEN ANDERSON

Woods Hole Oceanographic Institution, Woods Hole, Massachusetts

(Manuscript received 4 February 1994, in final form 18 June 1996)

ABSTRACT

Quasi-continuous depth–time observations of shear (5.5-m, 6-min resolution) and strain, ($\partial\eta/\partial z$, (2-m, 2.1-min resolution) obtained from the R/P *FLIP* are applied to a study of Richardson number (Ri) statistics. Data were collected off the coast of central California in the 1990 Surface Waves Processes Experiment. Observations are presented in Eulerian and in isopycnal-following frames. In both frames, shear variance is found to scale as $\overline{N^2}$ in the thermocline, in agreement with previous findings of Gargett et al. The probability density function for squared shear magnitude is very nearly exponential. Strain variance is approximately uniform with depth. The magnitude of the fluctuations is sufficient to influence the Ri field significantly at finescale.

To model the Richardson number, the detailed interrelationship between shear and strain must be specified. Two contrasting hypotheses are considered: One (H I) holds that fluctuations in the cross-isopycnal shear are independent of isopycnal separation. The other (H II) states that the cross-isopycnal velocity difference is the quantity that is independent of separation. Model probability density functions for Ri are developed under both hypotheses. The consideration of strain as well as shear in the Richardson calculation increases the probability of occurrence of both extremely low and high values of Ri. The observations confirm this general prediction. They also indicate that, while neither hypothesis is strictly correct, H II appears to be a much better approximation over the most commonly observed values of Ri.

1. Introduction

The dissipation of mechanical energy and the mixing of scalar quantities is found to occur in isolated patches in the ocean thermocline. Microscale turbulent motions initially derive their energy from larger (finescale 1–10 m) flows, which are prone to instability. The Richardson number, $\mathrm{Ri} = N^2/S^2$, where N^2 is the squared Väisälä frequency and $S^2 = (\partial u/\partial z)^2 + (\partial v/\partial z)^2$ is the squared shear, mediates one class of these instabilities (Miles 1961; Howard 1961). To predict the space–time variability of the Richardson number, the coevolution of the finescale shear and strain (N^2) fields must be understood.

The statistical modeling of the Richardson number has been addressed in pioneering studies by Bretherton (1969), Garrett and Munk (1972, hereafter GM72), Munk (1981, hereafter M81), and Desaubies and Smith (1982, hereafter DS82). Here we resume the discussion armed with

1) an improved statistical model for finescale strain, $\partial\eta/\partial z$ (where η is the vertical displacement of an isopycnal surface) and the resulting variations in Väisälä frequency (Pinkel and Anderson 1992, hereafter PA92)
2) new observations of shear and strain obtained from the Research Platform *FLIP* during the Surface Waves Processes Program (SWAPP). Coded pulse Doppler sonar (5.5-m vertical resolution over 45–300 m) and profiling CTDs (2-m vertical resolution, 720 profiles/day to 420 m) provide a fresh view of the upper-ocean shear and strain fields.

The modeling effort here differs from previous work in that:

- It is based on observations that are quasi-continuous in depth and time.
- The focus is shifted from a study of *the* gradient

Corresponding author address: Dr. Robert Pinkel, Marine Physical Laboratory, Scripps Institution of Oceanography, University of California, San Diego, La Jolla, CA 92093-0213.
E-mail: RPINKEL@UCSD.EDU

Richardson number to a study of the finite difference Richardson number Ri($\overline{\Delta z}$).

- The contribution of N^2 variability to the pdf of Ri is considered explicitly (as in DS82). While this contribution is not large at the ~10 m scales associated with most existing observations, its importance increases at the smaller scales more directly relevant to mixing processes.
- The distinction is made between statistical averages formed in Eulerian and isopycnal following (hereafter semi-Lagrangian or s-L) frames.

The Eulerian–semi-Lagrangian distinction is motivated by the observation (Fig. 1) that finescale shear is both advected and strained by the vertical motion of the internal wavefield. This is most easily seen in the depth range 80–200 m, where both the low frequency shear and high frequency internal waves are energetic. Typically, wave–shear interaction is discussed in terms of the refraction of high frequency waves by the shear associated with lower frequency motions (e.g., Bretherton 1966). Here we see that high frequency motions can significantly distort the lower frequency background. This observation is possible because the vertical resolution of the velocity observations is comparable to the typical vertical displacement scale of the internal waves. Self-deformation of the wavefield should be explicitly accounted for in any simple model of the Richardson number.

An introduction to the modeling of shear and strain is presented in section 2. Probability density functions (pdfs) of Richardson number are obtained as two-line derivations once the necessary groundwork is laid. The observations of shear, strain, and Richardson number are presented in section 3. Estimated pdfs of Ri are found to be in good agreement with model predictions.

The critical issue of the statistical independence of shear and strain is discussed in section 4. The various modeling options lead to significant differences in the pdfs for Richardson number, as well as differences in the values of statistical correlations that can be derived from the models.

2. A reversible finestructure approach to shear and strain modeling

Desaubies and Gregg (1981) first suggested that much of the finescale detail in vertical profiles of scalar properties is a consequence of the intense straining of the thermocline by the internal wavefield. They termed this deformation-related detail ''reversible fine structure.'' More recently, Pinkel and Anderson (1992) have adapted the reversible finestructure perspective in examining depth–time evolution of strain. A kinematic framework is defined whereby

isopycnal displacement

$$\eta(\rho, t) = z(\rho, t) - \overline{z(\rho)} \tag{1a}$$

isopycnal separation

$$\Delta z_{ij}(t) = z(\rho_i, t) - z(\rho_j, t) \tag{1b}$$

normalized separation

$$\gamma_{ij}(t) = \Delta z_{ij}(t)/\overline{\Delta z_{ij}} \tag{1c}$$

and

finite difference strain

$$\hat{\gamma}_{ij}(t) = \gamma_{ij}(t) - 1 \tag{1d}$$

are given in terms of the instantaneous depth $z(\rho,t)$ of an isopycnal surface of density ρ.

As a matter of notation, expected values of fluctuating quantities are denoted by angle brackets. The subscript $< >_E$ or $< >_L$ are used to specify the reference frame (Eulerian or semi-Lagrangian) in which the averages are accumulated. Basic-state variables are denoted by the overbar, for example, $\overline{z}\,(\rho)$, $\overline{\rho}(z)$, $\overline{N^2}(z)$. They correspond to averages formed in a wave-free environment. Distortion of the basic state by the motion field is represented multiplicatively, for example, $N^2(t) = \overline{N^2}\,\gamma^{-1}(t)$.

In an Eulerian frame, $\langle N^2\rangle_E = \overline{N^2}\langle\gamma^{-1}\rangle_E = \overline{N^2}$, rendering the definitions consistent. In a semi-Lagrangian frame, $\langle N^2\rangle_L = \overline{N^2}\langle\gamma^{-1}\rangle_L \geq \overline{N^2}$ (Pinkel et al. 1992).

In this work, with a focus on the variability of both shear and strain, it is of value to consider an s-L description of the horizontal velocity field $u_L(\rho,t)$. The motivations for this approach are dual. First, Anderson (1992) has observed that the time evolution of the horizontal velocity field is qualitatively more consistent with linear internal wave theory when viewed in an s-L frame than it is when viewed in the traditional Eulerian ($u_E(z,t)$) frame.[1]

Time evolution in an Eulerian frame has been termed ''contaminated'' by the presence of fine structure in instantaneous profiles of $\rho(z,t)$ and $u(z,t)$ (Phillips 1971; Garrett and Munk 1971; McKean 1974). The implication is that observations in an s-L frame are not contaminated. However, the existence of contamination in an Eulerian frame is no guarantee of apparent linear behavior in the s-L frame. Thus, Anderson's observation is of significance.

The second motivation for considering an s-L description of horizontal velocity stems from interest in the Richardson number (or alternatively, its inverse), which embraces both shear and strain (Väisälä frequency) fields. In the s-L description of finite differenced quantities, we have

[1] The two frames are related by $u_E(z_o,t) = u_L(\rho(z_o,t))$, where $\rho(z,t)$ is the inverse of $z(\rho,t)$. This inverse always exists in the reversible finestructure approximation as density is monotonic with depth.

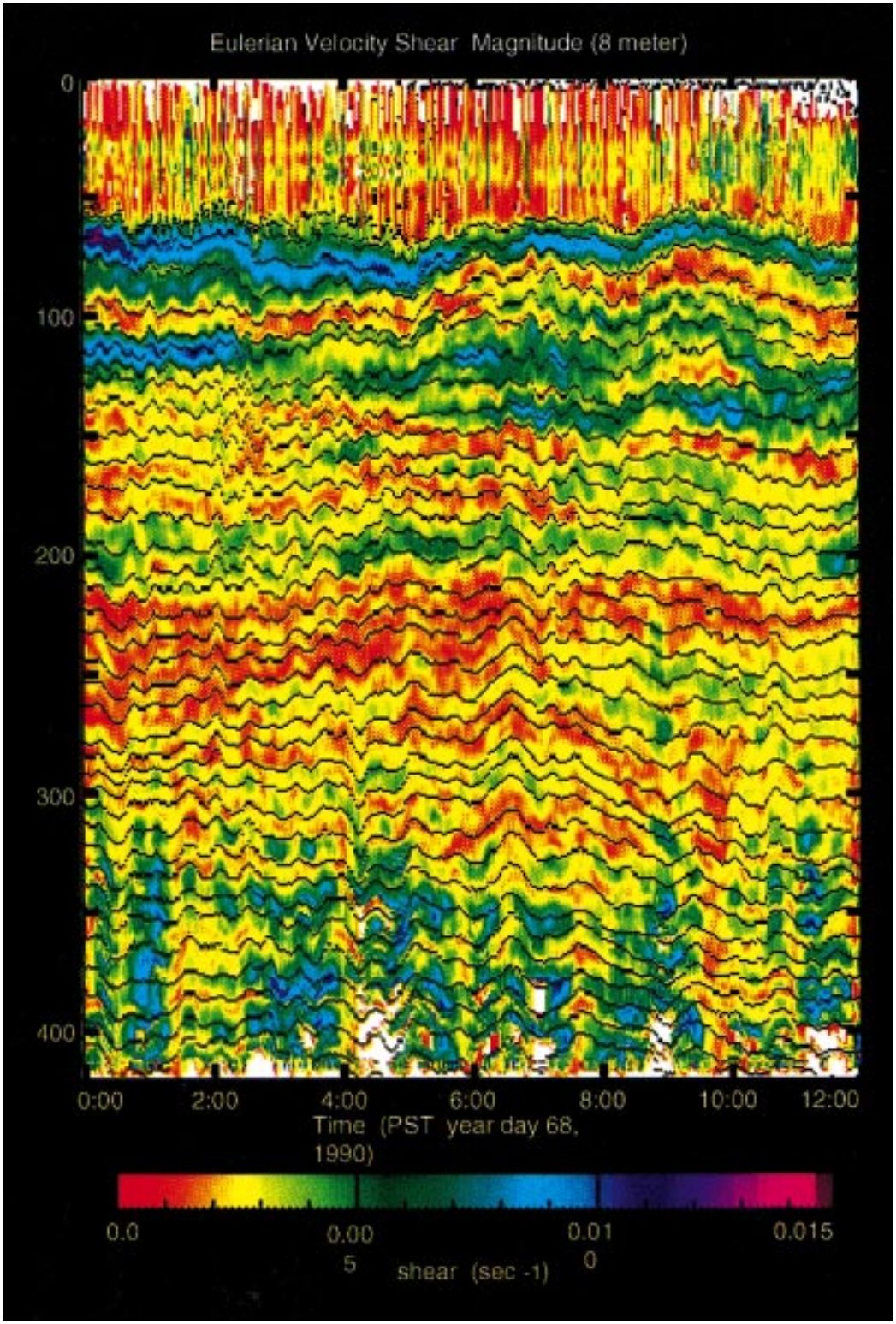

FIG. 1. A 12-h sample of shear magnitude $S = [(\partial u/\partial x)^2 + (\partial v/\partial y)^2]^{1/2}$ as estimated by the 161-kHz Doppler sonar. Colors represent shear magnitude. The solid lines give the depths of a selected set of isopycnals, as determined by the profiling CTD. Shear estimates in the upper mixed layer are corrupted by a variety of technical problems. Beyond 350 m, weak echoes result in degraded estimates. In the intervening region a clear picture of the shear field is seen. The shear field, in addition to influencing the propagation of high frequency waves, is also vertically advected by them.

$$N_{ij}^2(t) = \overline{N^2} \cdot \gamma_{ij}^{-1}(t) \quad (2)$$

$$S_{ij}(t) = (\Delta u_{ij}(t)/\overline{\Delta z_{ij}})\gamma_{ij}^{-1}(t). \quad (3)$$

Early modeling efforts (e.g., GM72, M81) considered only the role of shear variability in determining the value of the Richardson number. The Väisälä frequency was taken as a climatological constant. We term this the ''traditional model'' of the Richardson number

$$\mathrm{Ri}(t;\rho_i,\rho_j) = \overline{N^2}/S_{ij}^2(t) = \overline{\Delta z}_{ij}^2\ \overline{N^2}\ \gamma_{ij}^2(t)/\Delta u_{ij}^2(t). \quad (4)$$

If one wishes to extrapolate from large ($\sim$10 m) scales, where the traditional model is perhaps adequate, to smaller scales of more immediate relevance to the overturning process, Väisälä frequency fluctuations must be properly considered (DS82).

At this point, the issue of the statistical independence of shear and strain becomes central. DS82 assumed that shear squared fluctuations are in fact independent of fluctuations in strain. Presumably, cross-isopycnal differences in velocity, Δu_{ij}, adjust to changing isopycnal separation such that shear is unaffected. We refer to this as the hypothesis I (H I) model. An alternative hypothesis (H II) is that the velocity differences are themselves independent of isopycnal separation. The local shear squared is then dependent on strain. Clearly, if one of these plausible models is true, the other must be false. However, it is possible that *neither* of these limiting hypotheses is true (§ 4).

Quite different statistical models result from these contrasting hypotheses. If Ri is expressed as a product of statistically independent quantities, one has

$$\mathrm{Ri}_{\mathrm{I}} = \overline{N^2}/(S^2(t) \cdot \gamma(t)) \qquad \text{H I} \quad (5)$$

$$\mathrm{Ri}_{\mathrm{II}} = \overline{N^2}\ \overline{\Delta z}^2 \cdot \gamma(t)/\Delta u^2(t). \qquad \text{H II} \quad (6)$$

Interestingly, not all mean properties (such as the expected value of Ri) are sensitive to this fundamental issue. However, the nature of many important correlations (such as $\langle N^2 S^2\rangle$ or $\langle N^2 \mathrm{Ri}\rangle$) is strongly affected (appendix A).

This distinction between statistical models is not relevant when considering traditional Eulerian observations (e.g., Eriksen 1978). If velocity differences $\Delta u^2 \equiv (u(z_1) - (u(z_2))^2$ are independent of strain, then the squared shear $\Delta u^2/\overline{\Delta z}^2$ is as well.

PA92, however, introduce an alternative form of ''Eulerian'' average. As in an s-L study, they partition the thermocline using a set of isopycnal surfaces of mean separation $\overline{\Delta z}$. Rather than considering time averages along (or between) fixed isopycnals, they consider only that pair of isopycnals that bracket a fixed reference depth z_o. From realization to realization, the identity of the isopycnal pair changes. Pinkel and Anderson implied that, for passive scalars, such an Eulerian cross-isopycnal average is relevant to the traditional Eulerian finite difference over a vertical separation $\overline{\Delta z}$. When considering products of strained quantities, such as Ri, this is not the case. We can define an Eulerian average under H II in the sense of PA92, averaging Eq. (6) for isopycnals constrained to bracket a fixed reference depth. We term this average ''Eulerian II,'' or ''E II,'' and include an expression for the Eulerian II pdf of Richardson number below for completeness. The cross-isopycnal study required to verify its accuracy would be an interesting complement to traditional Eulerian observations.

In their earlier study DS82 modeled shear and strain as independent Gaussian quantities. Thus S^2 is described by the χ^2 probability density, which at two degrees of freedom (corresponding to the sum of the squares of the two shear components) has exponential form:

$$P(S^2) = \frac{1}{\langle S^2\rangle} e^{-S^2/\langle S^2\rangle} \quad (7a)$$

or

$$P(r) = e^{-r}, \quad (7b)$$

where $r \equiv S^2/\langle S^2\rangle$.

Recently, Gregg et al. (1993) have presented convincing evidence that, when statistics are accumulated in an Eulerian frame, 10-m differenced S^2 is well described by the χ^2 distribution. Their data were obtained from a free-fall vertical profiler. Statistical confidence was gained through averaging in depth rather than time at fixed depth/density (as here).

When considering statistics accumulated in an s-L frame, either S^2 or Δu^2 might be described by (7). Applying the SWAPP data to this issue, both variables are seen to exhibit near exponential pdfs. We proceed with the modeling, taking (7) for the pdf of both S^2 and Δu^2, as is convenient.

Modeling strain as a Gaussian quantity leads to potential difficulty. The Gaussian pdf admits the possibility that isopycnal surfaces can cross. This corresponds to an inversion in a density profile whose monotonicity is an inherent aspect of the reversible finestructure model. DS82 truncated their Gaussian pdf to prohibit the existence of density inversions.

More recently, PA92 identified the gamma pdf as appropriate for the description of strain statistics. Using CTD-derived isopycnal data (comparable to those described below), they found

$$P_L(\gamma) = \kappa(\kappa\gamma)^{\kappa-1}\ e^{-\kappa\gamma}/\Gamma(\kappa), \quad (8a)$$

$$P_E(\gamma) = (\kappa\gamma)^{\kappa}\ e^{-\kappa\gamma}/\Gamma(\kappa). \quad (8b)$$

Here $\kappa = \kappa_0\overline{\Delta z}$, where κ_0 is a constant of order 1.1 m^{-1}, and the subscripts L and E refer to the semi-Lagrangian and Eulerian frames. In addition to describing the data accurately, the gamma pdf is tractable analytically, as will be seen below.

It is convenient to introduce a scale Richardson number $\mathrm{Ri}^* = \overline{N^2}/\langle S^2\rangle$ (H I), or $\mathrm{Ri}^* = \overline{N^2}\,\overline{\Delta z}^2/\langle \Delta u^2\rangle$ (H II). The pdf of the normalized Richardson number $R = \mathrm{Ri}/\mathrm{Ri}^*$ and its inverse $R^{-1} = \mathrm{Ri}^{-1}\cdot\mathrm{Ri}^*$ can then be calculated, as a function of mean separation $\overline{\Delta z}$.

TABLE 1. Probability density functions of normalized Richardson number R = Ri/Ri* and inverse Richardson number as a function of normalized separation $\kappa = \kappa_0\overline{\Delta z}$.

Hypothesis I	Hypothesis II
S^2 is χ^2, independent of γ	Δu^2 is χ^2, independent of γ
$\mathrm{Ri}^*(\overline{\Delta z}) = \overline{N^2}/\langle s^2\rangle$	$\mathrm{Ri}^*(\overline{\Delta z}) = \overline{N^2}\ \overline{\Delta z}^2/\langle \Delta u^2\rangle$
s-L $P_{\mathrm{IL}}(R\,\vert\,\overline{\Delta z}) = \dfrac{2}{R\Gamma(\kappa)}\left(\dfrac{\kappa}{R}\right)^{(\kappa+1)/2} K_{\kappa-1}(\sqrt{\kappa/R})$	$P_{\mathrm{IIL}}(R\,\vert\,\overline{\Delta z}) = \dfrac{1}{R^2}\left[\dfrac{\kappa R}{\kappa R+1}\right]^{\kappa+1}$
Eulerian $P_{\mathrm{IE}}(R\,\vert\,\overline{\Delta z}) = \dfrac{2}{R^2\Gamma(\kappa)}\left(\dfrac{\kappa}{R}\right)^{\kappa/2} K_{\kappa}(\sqrt{\kappa/R})$	$P_{\mathrm{IIE}}(R\,\vert\,\overline{\Delta z}) = \dfrac{(\kappa+1)}{\kappa R^2}\left[\dfrac{\kappa R}{\kappa R+1}\right]^{\kappa+2}$
s-L $I_{\mathrm{IL}}(R^{-1}\,\vert\,\overline{\Delta z}) = \dfrac{2}{R^{-1}\Gamma(\kappa)}(\kappa R^{-1})^{(k+1)/2}\, K_{\kappa-1}(\sqrt{\kappa R^{-1}})$	$I_{\mathrm{IIL}}(R^{-1}\,\vert\,\overline{\Delta z}) = \left[\dfrac{1}{1+R^{-1}/\kappa}\right]^{\kappa+1}$
Eulerian $I_{\mathrm{IE}}(R^{-1}\,\vert\,\overline{\Delta z}) = \dfrac{2}{\Gamma(\kappa)}(\kappa R^{-1})^{\kappa/2}\, K(2\sqrt{\kappa R^{-1}})$	$I_{\mathrm{IIE}}(R^{-1}\,\vert\,\overline{\Delta z}) = \dfrac{\kappa+1}{\kappa}\left[\dfrac{1}{1+R^{-1}/\kappa}\right]^{\kappa+2}$

Applying the scale Richardson number to expressions (5) and (6), one obtains

$$R = (r_{\mathrm{I}}\gamma)^{-1} \qquad \text{H I} \qquad (9a)$$
$$r_{\mathrm{I}} \equiv S^2/\langle S^2\rangle$$
$$R = r_{\mathrm{II}}^{-1}\gamma \qquad \text{H II} \qquad (9b)$$
$$r_{\mathrm{II}} \equiv \Delta u^2/\langle \Delta u^2\rangle$$

The present task is to produce model pdfs of these expressions, given the accepted expressions [Eqs. (7) and (8)] for r and γ variability. At this point, it is a textbook problem.

Given two independent random variables, a and b, with joint probability density $\mathrm{P(a,b)} = P_a(a)P_b(b)$, the probability density of the ratio $c = a/b$ is

$$P_c(c) = \int_0^\infty |b| P_a(cb)P_b(b)\, db \qquad (10)$$

(Papoulis 1984).

We apply this result to (9a), first introducing $g = r^{-1}$ with *pdf* $G(g) = g^{-2}e^{-1/g}$. We have for the s-L case

$$P_{\mathrm{IL}}(R\,\vert\,\overline{\Delta z}) = \int_0^\infty \gamma\left[\frac{1}{\gamma^2R^2}e^{-1/R\gamma}\right]\left[\kappa\frac{(\kappa\gamma)^{\kappa-1}}{\Gamma(\kappa)}e^{-\kappa\gamma}\right] d\gamma. \qquad (11)$$

This integral is evaluated in terms of the modified Bessel function κ_Δ (e.g., Prudnikov et al. 1986, integral 2.3.16: 1), yielding

$$P_{\mathrm{IL}}(R\,\vert\,\overline{\Delta z}) = \frac{2}{R\Gamma(\kappa)}\left(\frac{\kappa}{R}\right)^{(\kappa+1)/2} K_{\kappa-1}(2\sqrt{\kappa/R}). \qquad (12)$$

Expressions for the pdf in an Eulerian frame, as well as for pdfs of inverse Richardson number, are presented in Table 1.

Under H II, Δu^2 is a χ^2 random variable that is presumed independent of strain. Applying (10) to (9b) we have, in the s-L case,

$$P_{\mathrm{IIL}}(R\,\vert\,\overline{\Delta z}) = \int r[e^{-r}][\kappa(\kappa Rr)^{\kappa-1}e^{-\kappa Rr}/\Gamma(\kappa)]\, dr. \qquad (13)$$

This integral is easily evaluated, yielding

$$P_{\mathrm{IIL}}\ (R\,\vert\,\overline{\Delta z}) = \frac{\kappa}{R(\kappa R+1)}\left[\frac{\kappa R}{\kappa R+1}\right]^{\kappa}. \qquad (14)$$

Corresponding expressions for the Eulerian pdf as well as pdfs of inverse Richardson number are presented in Table 1.

Note that the vertical scale enters these expressions in two ways. First, $\kappa = \kappa_0\overline{\Delta z}$. Also, the scale Richardson number Ri* depends on the finite difference of either $\langle S^2\rangle$ (H I) or $\langle \Delta u^2\rangle$ (H II). Both are dependent on $\overline{\Delta z}$.

The pdfs derived under H I and H II are plotted in Figs. 2a, b. Several aspects of these plots deserve comment. First, the differences between observations in the s-L and Eulerian frames are quite significant at small mean separations. The differences diminish rapidly as separation increases. For $\kappa > 12$ it will be challenging to detect differences between reference frames experimentally.

Under H I, (S^2 and N^2 are independent), the Eulerian pdf is more skewed than its s-L counterpart. Differences diminish with increasing mean separation $\kappa_0\overline{\Delta z}$. Under H II, the Eulerian pdf for Ri is identical to its H I form. However, the s-L pdf now has a greater skewness than the Eulerian (2b). While the differences between the s-L and true Eulerian observations are slight, they do not diminish at large differencing scales. In contrast, the differences between the Eulerian II (where statistics are accumulated between isopycnal pairs constrained to bracket fixed reference depths) and s-L models are significant at small κ, decreasing substantially as κ increases.

It is also apparent in Fig. 2 that extremely low values of R occur less frequently under H I than H II. To investigate statistical behavior at small R, it is attractive to consider pdfs of normalized inverse Richardson number $R^{-1} \equiv \mathrm{Ri}^{-1}\mathrm{Ri}^*$ (Fig. 3, Table 1). For reference, the

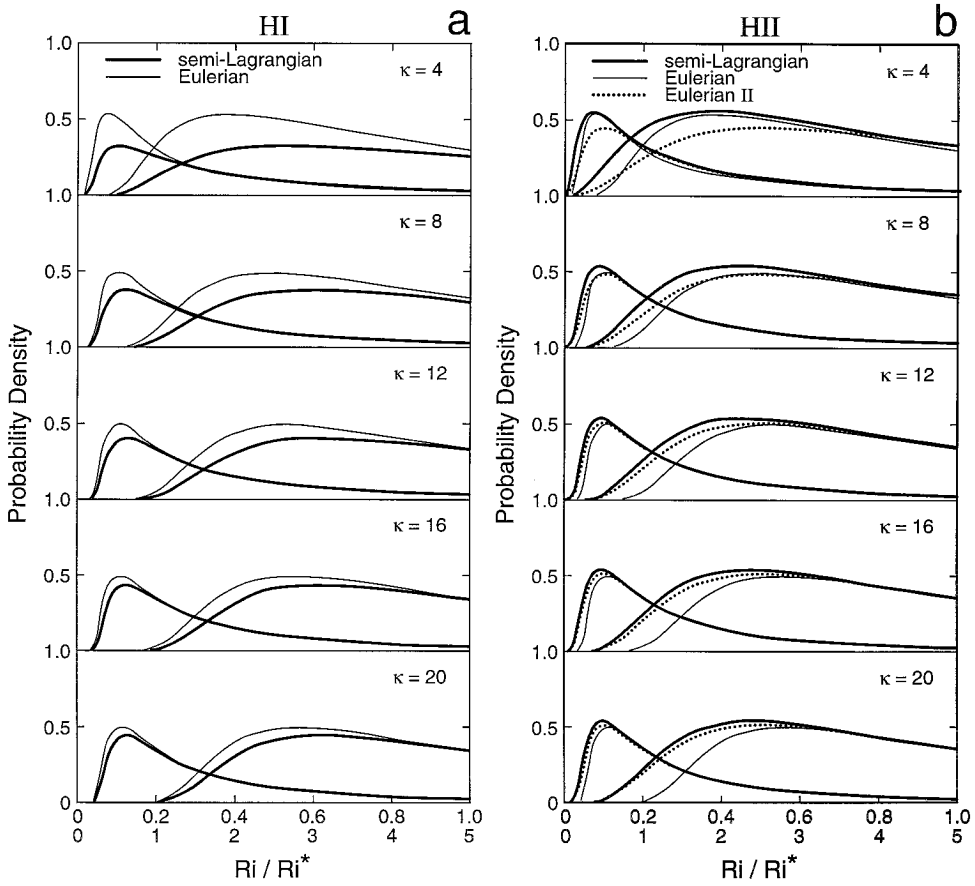

FIG. 2. Model probability density functions of Richardson number derived under hypotheses I (a) and II (b). The full pdfs are plotted over the range $R = \mathrm{Ri}/\mathrm{Ri}^* = 0 - 5$. An enlargement of the low Richardson number $R < 1$ portion of the pdf is overplotted, to enable detailed examination of the differences. Under H II, an Eulerian average is formally identical to that under H I. One can define an alternative Eulerian average, embracing cross-isopycnal differences (§ 2). For completeness we present the alternative Eulerian model in (b) termed Eulerian II, as well as the standard Eulerian result.

pdf of the ''traditional'' inverse Richardson number is also plotted. Since only variations in S^2 are considered, the traditional pdf is exponential (Anderson 1992; Polzin 1992).

It is seen that, relative to the traditional model, there are more occurrences of extremely large and extremely small R^{-1} when the effects of strain are considered. For example, at $\kappa = 4$ (Fig. 3a) an Eulerian ''$R^{-1} = 5$'' occurrence is more than twice as likely when strain is considered versus neglected. A similar situation exists under H II in the s-L frame (Fig. 3c). As one progresses to larger mean separations (Figs. 3b, 3d), the significance of strain diminishes and all models approach the traditional exponential form.

3. Observations

In February and March 1990, the Research Platform *FLIP* was trimoored at 35°N, 127°W, collecting data in support of the Surface Waves Processes Program (SWAPP). The experiment site was in water 4 km deep, approximately 600 km west of Pt. Conception, California. The mean Väisälä profile at the site is given in Fig. 4. As an aspect of this effort, two profiling CTDs and a downlooking Doppler sonar were operated. The CTDs, Seabird Instruments SBE-9, profiled at 130-s intervals from 2 to 220 m (upper) and 200 to 420 m (lower). The fall rate of the instruments was approximately 3.5 m s^{-1}. At this speed it was not necessary to pump the conductivity cells to achieve adequate temporal response. To minimize ''salinity spiking,'' the conductivity data required response correction. A section of test data of nearly uniform salinity was selected. The transfer function between the temperature gradient and conductivity gradient was estimated for this section. This transfer function was then used to ''match'' the conductivity data to the temperature signal throughout the depth–time domain of the experiment. Both the temperature and corrected conductivity signals were low-pass filtered (1.6-m

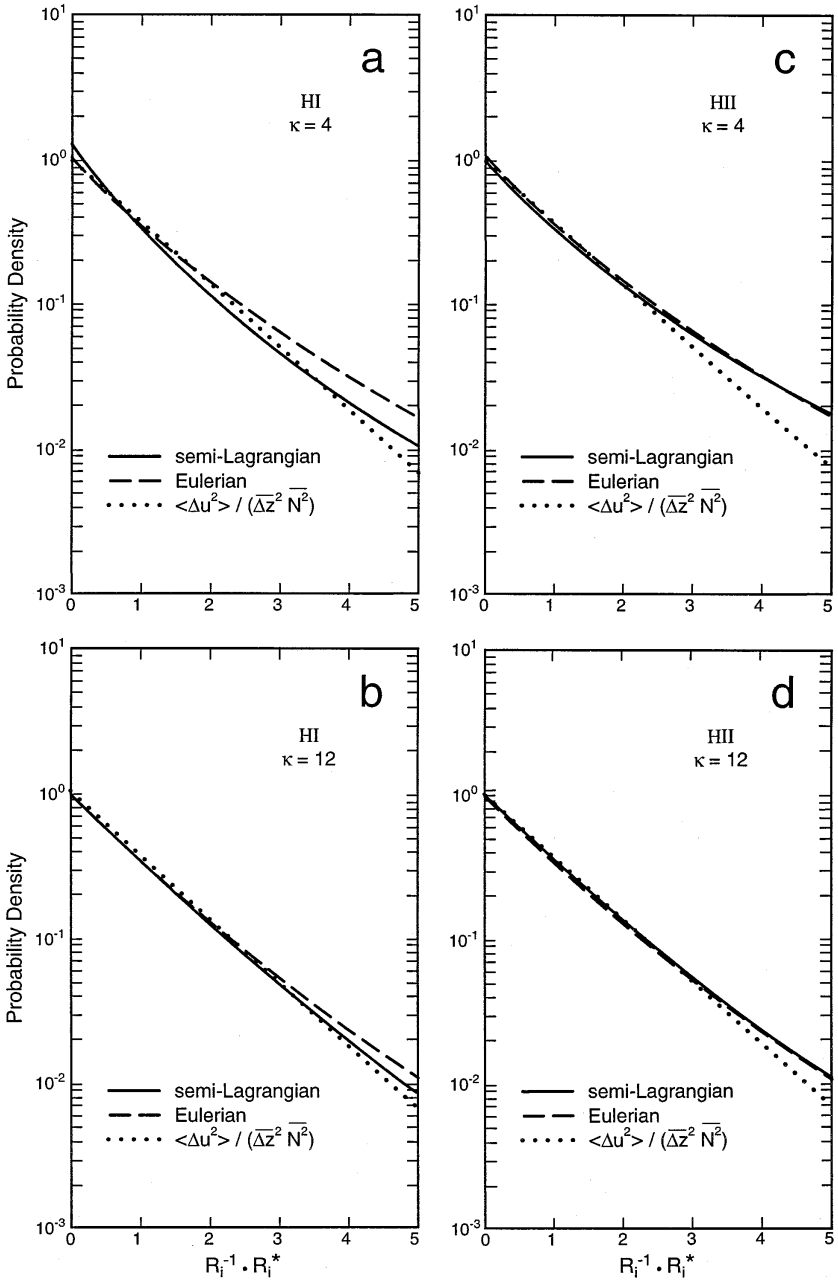

FIG. 3. Model probability density functions of R^{-1} = Ri^{-1} * Ri*. Models are derived under H I (a, b) and H II (c, d). The traditional exponential model is plotted as a reference.

cutoff) prior to the calculation of density. The procedure is discussed in more detail in Anderson (1992) and Sherman (1989).

The Doppler sonar used in this study was a 161-kHz four beam device constructed at the Marine Physical Laboratory of Scripps. Originally designed for Arctic research, the system was here mounted on *FLIP*'s hull at a depth of approximately 15 m. A repeat sequence code (Pinkel and Smith 1992) consisting of six repeats of a 7-bit Barker code was transmitted. The bandwidth of the code was 5 kHz. The associated vertical resolution of the sonar was 5.5 m. The theoretical velocity precision of the instrument was 0.74 cm s^{-1} after one minute of averaging, as limited by the performance of the code. In fact, the dominant limit to precision was the surface wavefield, which moved both the upper ocean and *FLIP* at speeds far greater than typical thermocline velocities. Six-minute average velocity profiles (30 periods of a 12 second wave) were subsequently formed in an effort to reduce the ''wave noise'' in our signals.

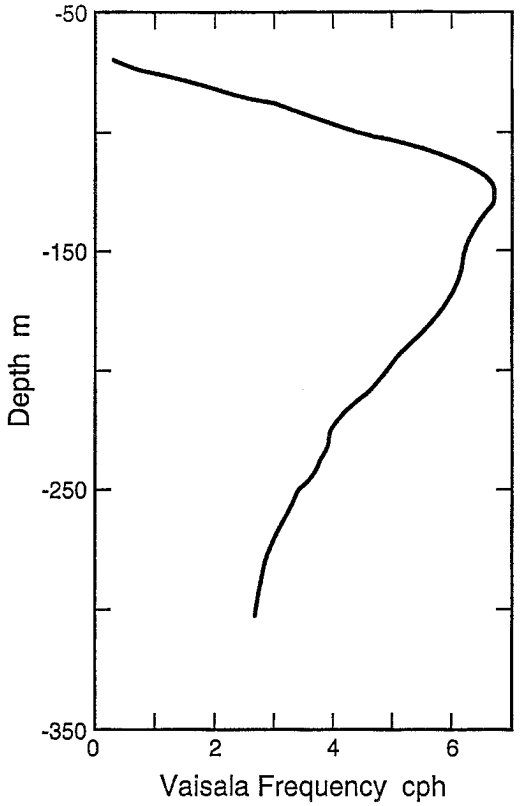

FIG. 4. The SWAPP mean Väisälä profile.

Issues of resolution and precision are further discussed in appendix B.

SWAPP was sited in a region of both surface and subsurface frontal activity. Energetic subinertial features were present in the upper 120 m early in the experiment. Later, yeardays 67–70 (8–11 March), a major subsurface front was seen at 200–300 m (Anderson 1992). To minimize influence of these thermohaline features, a subset of the overall observations was selected for the Richardson number study. Analysis efforts focus on the depth region 150–250 m over the first 7.5 days of the experiment, days 60–67.5 (1–8 March).

In restricting the data to avoid ''anomalous'' conditions the statistical precision of the results was reduced. Specifically, the subset extended over only 8 periods of the dominant near-inertial shear, and 1–2 dominant wavelengths in depth. The bandwidth of the near-inertial field was sufficiently narrow that relatively few independent realizations of the shear (and strain) process were captured. Briscoe (1977) suggested an 11-h interval is required between independent shear observations, based on data obtained at 28°N. Thus, the statistical stability of the SWAPP probability estimates was limited. However, relative to previous 1-d time series or vertical profiles, the present 2-d observations represent an advance.

Climatologically, the overall SWAPP shear variance was 1.3 times the Garrett–Munk (1975) nominal value. During the first week of the experiment, however, shear variance was low, approximately 50% of GM75. Strain variance was also reduced relative to G–M by a factor of .75 (Anderson 1992). The strain scaling constant κ_0 has a value of 2 m^{-1} for the SWAPP observation, in contrast to the suggested ''canonical'' value of 1.2 m^{-1} (PA92).

Probability density functions of strain formed in an s-L frame closely resemble the Gamma pdf, scaled as suggested by PA92. Pdfs formed in an Eulerian frame were significantly influenced by the vertical advection of subinertial features. A basic tenet of the reversible fine structure model is that, in the absence of straining, underlying scalar property profiles are smooth. This is not the case here. While fixed irregularities can be accounted for in the modeling, for simplicity we will focus on the comparison of the s-L model pdfs and the corresponding s-L observations.

a. Vertical variability of shear variance and mean Richardson number

As an initial study, profiles of mean square shear and inverse Richardson number are formed over the depth range 120–296 m (below the $\overline{N^2}$ maximum). We plot these as a function of $\overline{N^2}(z)$, rather than depth itself, to investigate their scaling behavior.

In Fig. 5a, finite difference shear variance, uncorrected for sonar resolution, is plotted as a function of $\overline{N^2}$. Averages are formed in both Eulerian and semi-Lagrangian frames. Typically the s-L averages exhibit slightly greater variance. In spite of significant variability, the shear variance in both frames appears to scale linearly with $\overline{N^2}$, consistent with previous findings (e.g., Gargett et al. 1981).

In Fig. 5b, the s-L shear variance is compared with the related quantity, the variance of the s-L velocity difference, $\Delta u^2\ (t,\rho_i,\rho_j)$, normalized by the square of the mean isopycnal separation. The variance profiles are nearly congruent at the 18- and 10-m mean separations. At 6 m, there is some indication of enhanced variance of true shear relative to $\langle \Delta u^2 \rangle / \overline{\Delta z^2}$ at depth.

Profiles of mean inverse Richardson number $\langle S^2/N^2 \rangle$ are presented in Fig. 6. In addition to the s-L and E II averages, profiles of the ''traditional'' buoyancy normalized shear variance $\langle S^2 \rangle / \overline{N^2}$ are also presented, averaged in an Eulerian frame. These inverse Richardson number estimates are far from critical, varying from .2 to .4 as spatial separations decrease from 18 to 6 m. The estimates appear approximately independent of Väisälä frequency. The profiles are sufficiently irregular with depth that weak dependencies cannot be detected.

b. Shear variance and Richardson number as a function of vertical differencing scale

A second issue is the rate at which shear variance decreases with increasing mean isopycnal separation

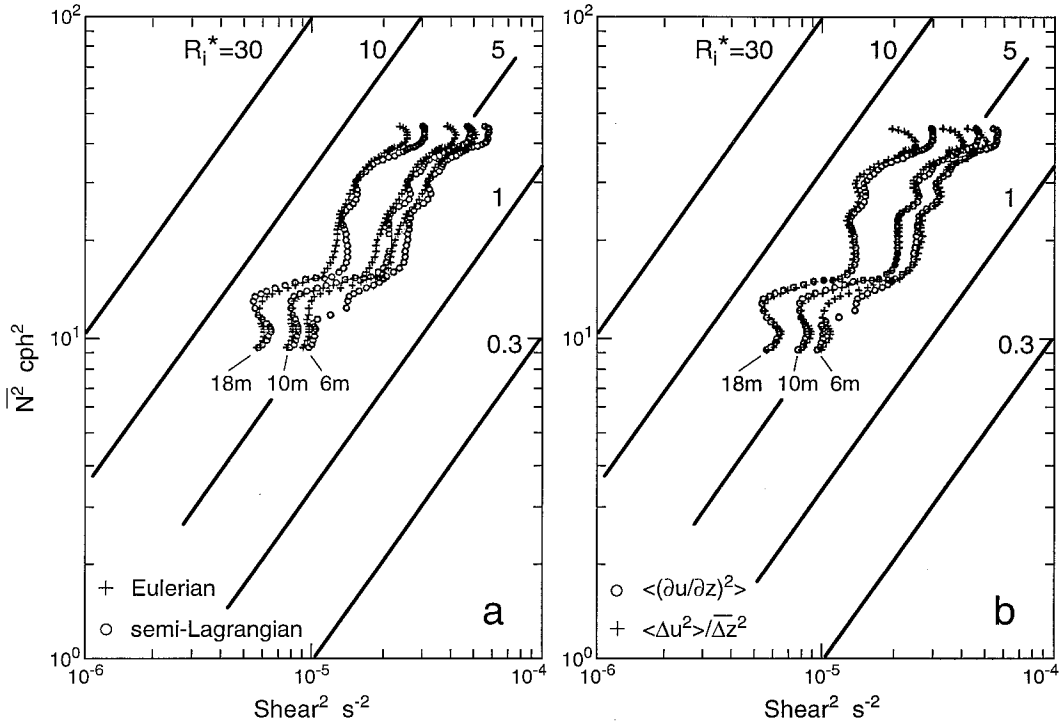

FIG. 5. Plot of $\langle S^2 \rangle$ as a function of Väisälä frequency at mean vertical differencing intervals of 6, 10, and 18 m. Lines of scale Richardson number are drawn for reference. In (a) Eulerian and semi-Lagrangian averages are compared. In (b) true s-L shear is compared with the normalized velocity difference $\langle \Delta u^2 \rangle / \overline{\Delta z}^2$. Profiles are computed without correction for instrument resolution and noise, using data from below 120 m.

(s-L) or differencing interval. This is examined in Fig. 7a for data obtained at 150- and 250-m mean depths. Independent of reference frame or data type, shear variance decreases with increasing vertical mean separation, approaching a Δz^{-1} dependence at separations greater than 10 m for the shallow data. The deep data appear to undergo this transition more gradually, a fact generally consistent with WKB scaling and inconsistent with the empirical dictum that the vertical wavenumber spectrum of shear does not change form with depth (Gargett et al. 1981).

A major concern is that both noise and the finite resolution of the sonar affect these results. These processes are modeled in appendix B. A comparison of the 150-m data, uncorrected and ''corrected'' for resolution and noise is presented in Fig. 7b. Here it is assumed that the rms noise in a given sample of sonar data is 1 cm s^{-1} and that the true shear spectrum is as given in Gargett et al. (1981). While the ultimate Δz^{-1} dependence of shear variance is unaffected by noise and resolution, changes at small vertical differencing intervals are significant. A 2-m first difference shear variance estimate obtained from a noise-free sensor of extremely high resolution would be approximately a factor of 1.8 greater than the SWAPP sonar estimate. When considering differencing intervals of 6 m and above, the effects are considerably more modest. Nevertheless, Fig. 7b clearly suggests that much can be gained by developing instruments of improved precision and resolution. Corresponding plots of inverse Richardson number are presented in Figs. 8a,b. Estimates of Ri^{-1} at 250 m are uniformly less than their 150-m counterparts (8a). The difference increases with decreasing mean separation. To the extent that mean values of $\mathrm{Ri}^{-1}(\overline{\Delta z})$ vary with depth, the variation will be most apparent at small $\overline{\Delta z}$. The enhanced depth variability at 6-m mean separation relative to that at 10 and 18 m could be seen more clearly in Fig. 6 if the abscissa were plotted on a linear scale.

As with the straight shear estimates, sonar noise and resolution significantly affect the inverse Ri estimates at small mean separations. In Fig. 8b the variation of the inverse Richardson number is plotted versus mean separation for 150-m data. Also plotted is a second set of estimates, where shear variance is enhanced to correct for finite sonar resolution and reduced to account for the expected noise level (appendix B). The correction is significant for scales below 10 m. Even as corrected, the inverse Richardson number falls short of Munk's (1981) hypothesized value of unity at 10-m vertical scales by a factor of 50%. Relative to the stability of the thermocline, shears in the early part of SWAPP were mild.

c. Probability density functions of R and R^{-1}

Probability density functions of R and R^{-1} were formed and averaged (in an s-L frame) over yeardays

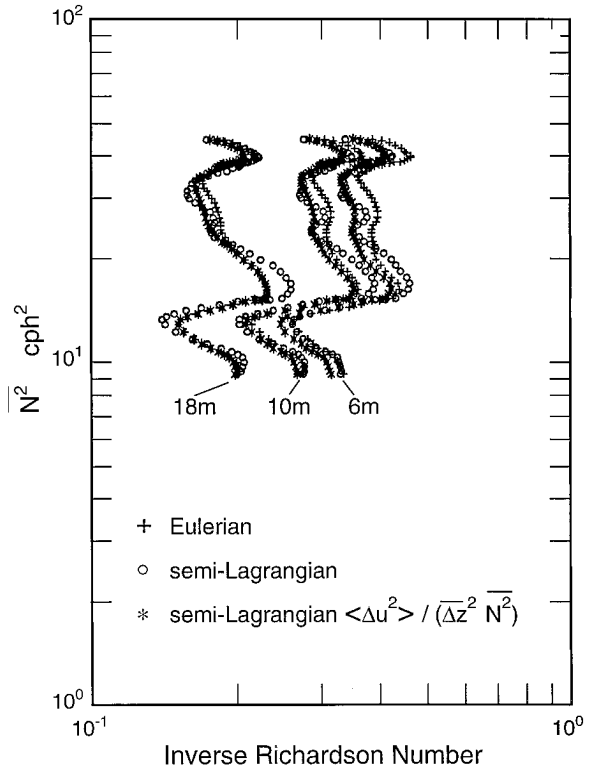

FIG. 6. The expected value of inverse Richardson number plotted as a function of $\overline{N^2}$. These profiles are computed without correction for instrument resolution and noise, using data from below 120 m.

60–67.5, depths 150–200 m. The restricted sampling substantially avoids observed frontal activity. Observed pdfs are compared with modeled forms (section 2) in Fig. 9. The comparison is conducted for mean separation of 6, 10, and 18 m. Values of Ri* are determined from the 50-m average of $\langle S^2 \rangle$ or $\langle \Delta u^2 \rangle$. Other than the observed shear variance and the strain parameter $\kappa_0 = \kappa / \overline{\Delta z}$, which is assigned the value 2 m^{-1} for all observations, there are no adjustable parameters in these fits.

In general, the H II model (Δu^2 independent of strain) does a better job of fitting the observations for commonly observed values of R. The model is slightly skewed relative to the observations at $\overline{\Delta z} = 6m$, (Fig. 9a), overpredicting the occurrence of small R events. The H I model severely underestimates the peak value of the observed pdfs.

The observed pdfs of inverse Richardson number $R^{-1} = \mathrm{Ri}^{-1}\, R^*$ emphasize the regions where instability can be expected. In Figs. 9d–f, the logarithm of the pdf is plotted in an attempt to focus on the incidence of large R^{-1} occurrences. Reference lines for the H I, H II, and traditional models are drawn. Unusually large R^{-1} events occur more frequently than are predicted by the traditional model, particularly at small separation. The H I model is generally more consistent with the observations in this region. The H II model overpredicts relative to the observations.

We note, that the pdf estimates are significantly ''data starved'' at large R^{-1}. Accurate estimates of the value

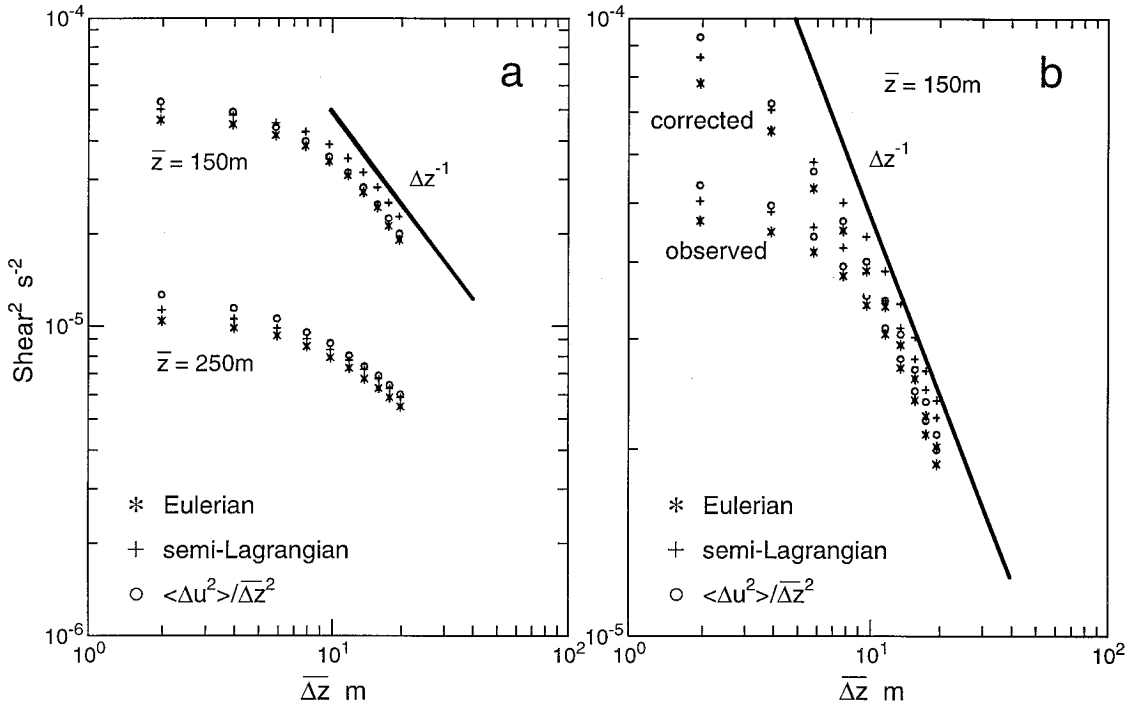

FIG. 7. Finite difference $\langle S^2 \rangle$ as a function of the mean differencing interval $\overline{\Delta z}$. In (a) estimates are centered on depths of 150 and 250 m. In (b) the 150-m averages are shown, as calculated from the raw data and following corrections for instrument noise and resolution (appendix B). An rms error of 1.0 cm s^{-1} is assumed for the velocity.

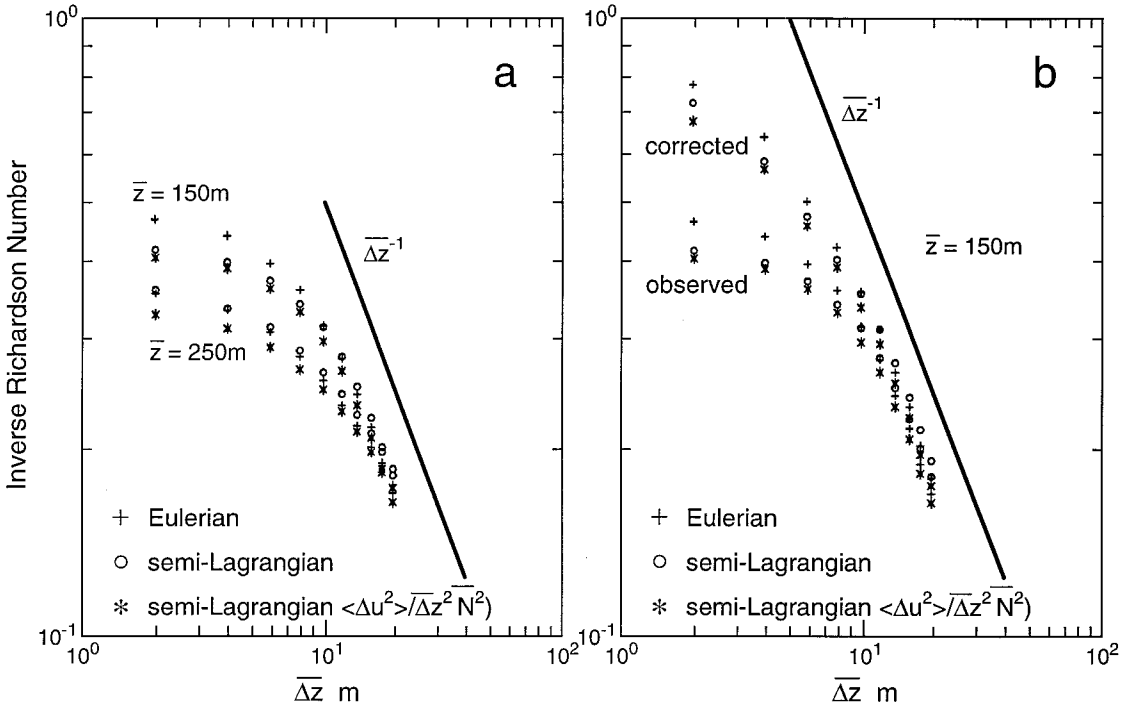

FIG. 8. The expected value of inverse Richardson number as a function of the mean differencing interval $\overline{\Delta z}$ used in the shear and strain calculations. Estimates are presented (a) at observed depths of 150 and 250 m and (b) as corrected for sonar noise and resolution (appendix B). An rms velocity error of 1 cm s^{-1} is assumed for the correction.

of the pdf governing these extremely rare events require longer data records and/or higher-resolution (larger Ri*) sensors.

4. The statistical independence of shear squared and N^2

The independence of S^2 and N^2 is an issue central to both the statistics and the dynamics of the finescale fields. To explore this matter, the joint probability density function of S^2 and N^2 can be formed in both Eulerian and s-L frames. Additionally, the joint pdf of cross-isopycnal squared velocity Δu^2, and N^2 can be generated (Fig. 10). The joint pdfs are formed over 100 × 100 bins in r and γ^{-1}. Figure 10 is further smoothed using a 3 × 3 bin convolution to aid in visualization. Distinct from the pronounced central peak, a ridge of the pdf extends to high S^2 values along $\gamma^{-1} = .05 - 1$ (N^2 slightly less than average). A second, less visible ridge extends to high values of N^2 along $r = 0$. This ''two-armed'' form for the joint pdf cannot be expressed as a product of univariate pdfs for N^2 and Δu^2. This precludes the statistical independence of these quantities.

The apparent ridges in the pdf describe the occurrence of *rare* events. The *typical* behavior of the thermocline can be investigated using the correlation between the observed Δu^2 (or S^2) and N^2:

$$C(\overline{\Delta z}) = \frac{\langle S^2 \cdot N^2\rangle - \langle S^2\rangle\langle N^2\rangle}{(\langle S^4\rangle - \langle S^2\rangle^2)^{1/2}\,(\langle N^4\rangle - \langle N^2\rangle^2)^{1/2}} \quad (15)$$

Estimates of the correlation are presented as a function of mean separation in Fig. 11. Significant correlation precludes statistical independence.

Surprisingly, the observed correlations between S^2 and N^2 are large, in spite of the fact that N^2 variations are relatively weak over much of the range of $\overline{\Delta z}$ investigated. At 2-m mean separation, the correlations are .2–.4 in the s-L frame, .3–.5 in the Eulerian frame. With increasing mean separation, the correlation grows slightly in both frames. In contrast, the correlation between Δu^2 and N^2 is weakly negative ($-.2$) at the smallest separations. It grows toward zero as separation increases.

The strong S^2–N^2 correlation significantly complicates efforts to model Richardson number statistics. Several processes that contribute to this correlation can be identified:

(i) If, in the s-L frame, it really is the case that Δu^2 is independent of N^2, then the covariance of S^2 and N^2 is given by

$$\begin{aligned}\mathrm{cov}(S^2,N^2) &= \langle S^2N^2\rangle - \langle S^2\rangle\langle N^2\rangle \\ &= \left\langle \frac{\Delta u^2}{\overline{\Delta z^2}}\gamma^{-2}\cdot\overline{N^2}\gamma^{-1}\right\rangle - \left\langle \frac{\Delta u^2}{\overline{\Delta z^2}}\gamma^{-2}\right\rangle\cdot\overline{N^2}\langle\gamma^{-1}\rangle \\ &= \langle\Delta u^2\rangle\overline{N^2}/\overline{\Delta z^2}\;[\langle\gamma^{-3}\rangle - \langle\gamma^{-2}\rangle\langle\gamma^{-1}\rangle] > 0.\end{aligned} \quad (16)$$

The quantities necessary to evaluate this covariance

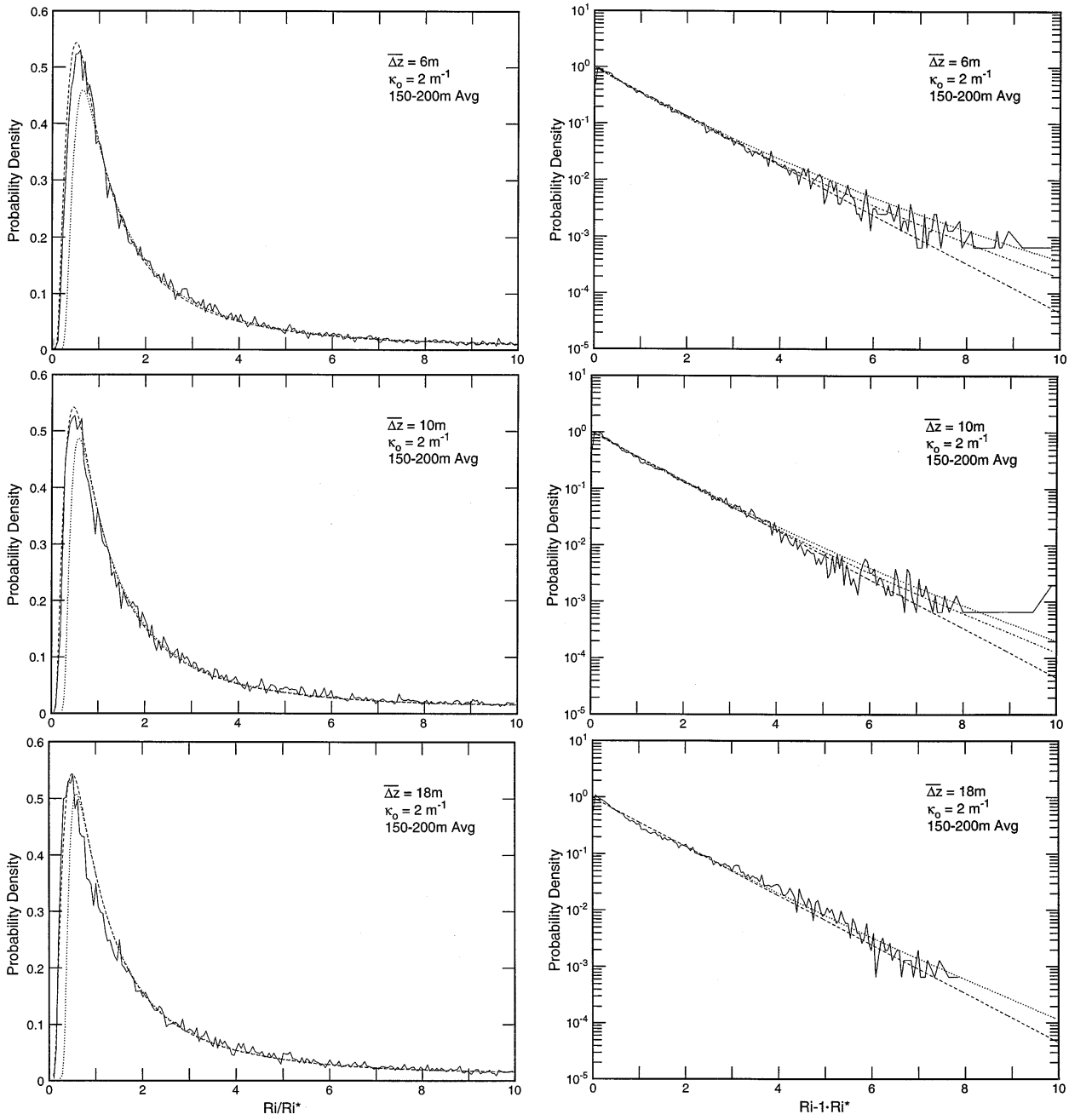

FIG. 9. Model probability density functions of R (a)–(c) and R^{-1} (d)–(f), compared with SWAPP 150–200-m s-L data. With $\kappa_0 = 2\ m^{-1}$ established for the entire dataset, the shear variance is the only free model parameter at each separation. These fits are accomplished with the model variance set to the observed values. The H II models (dashed lines) describe the observations better than the H I models (dotted lines) at commonly experienced values of R, R^{-1}.

can be easily calculated from model pdfs presented in PA92, (or appendix A, here).

(ii) Variations in the ''background'' N^2 profile refract internal waves as they propagate vertically. Regions of high S^2 can be expected in regions of high N^2, in a WKB approximation of the refraction process.

Climatologically, both $\overline{N^2}$ and $\langle S^2 \rangle$ decrease with depth (below 120 m). Crests of internal waves lift regions of low $\langle N^2 \rangle_L$, $\langle S^2 \rangle_L$ water up to a fixed reference depth. Troughs bring regions of high $\langle N^2 \rangle_L$, $\langle S^2 \rangle_L$ water down from above. A strong positive $\langle N^2 S^2 \rangle_E$ covariance can be expected if $\langle\ \rangle_E$ corresponds to a time average at fixed depth.

It is important to note that an Eulerian *depth* average, such as might be obtained from an instrument that makes isolated vertical profiles, would not see an apparent co-

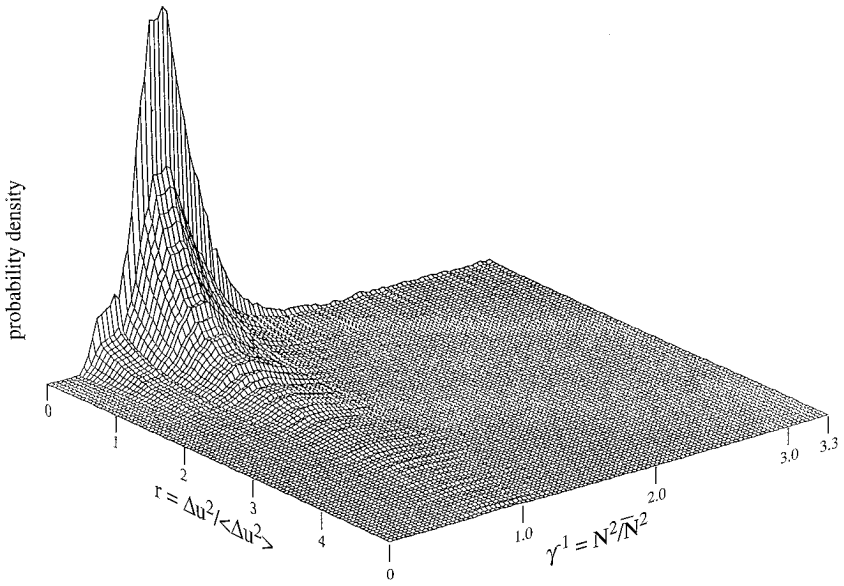

FIG. 10. An estimate of the joint probability density function of Δu^2 and N^2. Estimates are formed with a mean differencing interval of 10 m using data from 150–200 m.

variance caused by vertical advection. Nevertheless, significant coherences between N^2 and S^2 have been observed (Rubenstein et al. 1982; Evans 1982). Vertical advection is not the sole cause of the Eulerian correlation. Our observed correlation in the S-L frame supports this conclusion.

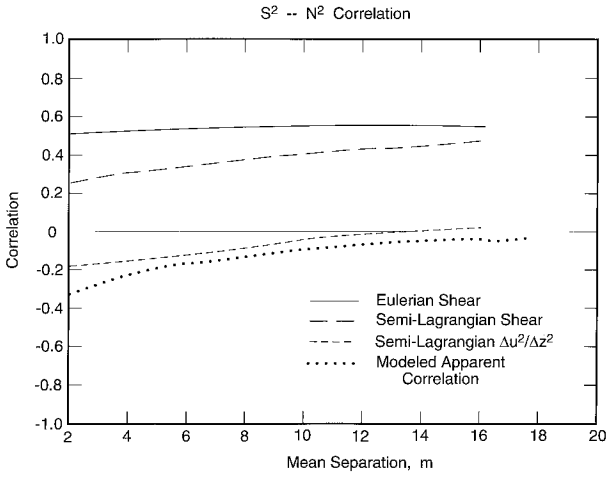

FIG. 11. The observed correlation between squared shear and Väisälä frequency for the depth range 150–200 m. The Eulerian correlation is positive and relatively independent of spatial lag. The vertical advection of the mean S^2 and N^2 fields, both of which decrease with increasing depth, might account for a significant fraction of this correlation. Semi-Lagrangian estimates experience advective effects differently. Again, a positive correlation is observed whose magnitude increases with increasing mean separation. In contrast, estimates of the correlation of $\Delta u^2 - N^2$ in an s-L frame are weakly negative at small lag, increasing toward zero as the lag increases. A model describing the effect of finite sonar resolution on the correlation estimate (appendix B) produces a qualitatively similar result.

The strong correlation between S^2 and N^2 convincingly refutes hypothesis I, that the quantities are statistically independent. From a modeling perspective, it would be extremely attractive for hypothesis II to be valid. Otherwise, additional physical information is required to fully describe the observations. It is thus disturbing to see the negative correlation between Δu^2 and N^2 in Fig. 11.

We suggest that this correlation is in part due to the finite resolution of the Doppler sonar. When a given pair of isopycnals is close together—relative to the resolution of the sonar—the estimated value of Δu^2 will be less than the actual value. When the same pair is widely separated, the Δu^2 values will be unbiased. Thus, a tendency for low Δu^2 to be associated with high N^2 can result from finite sonar resolution. An apparent negative correlation is created. This apparent correlation is easily modeled (appendix B) and is plotted in Fig. 11 as a reference line. The observed correlation is well described by the model, except perhaps at those lags so small that the finite resolution of the CTD becomes significant.

The preliminary correlation analysis is consistent with the hypothesis that Δu^2 and N^2 are independent quantities, while S^2 and N^2 are not. However, visual inspection of the joint pdf (Fig. 10) suggests a more complicated picture. As a metric of the ''degree'' of independence of shear and strain we can apply the joint pdfs to estimate $\langle S^2 \rangle$ or $\langle \Delta u^2 \rangle$ at each value of γ^{-1}. If the fields are statistically independent, the observed $\langle S^2 \rangle(\gamma^{-1})$ or $\langle \Delta u^2 \rangle(\gamma^{-1})$ will be independent of γ^{-1}, as well. These estimates, normalized by the overall $\langle S^2 \rangle, \langle \Delta u^2 \rangle$ are presented in Figs. 12 a–c. The pdfs of γ^{-1} are overplotted to give some indication of the relative

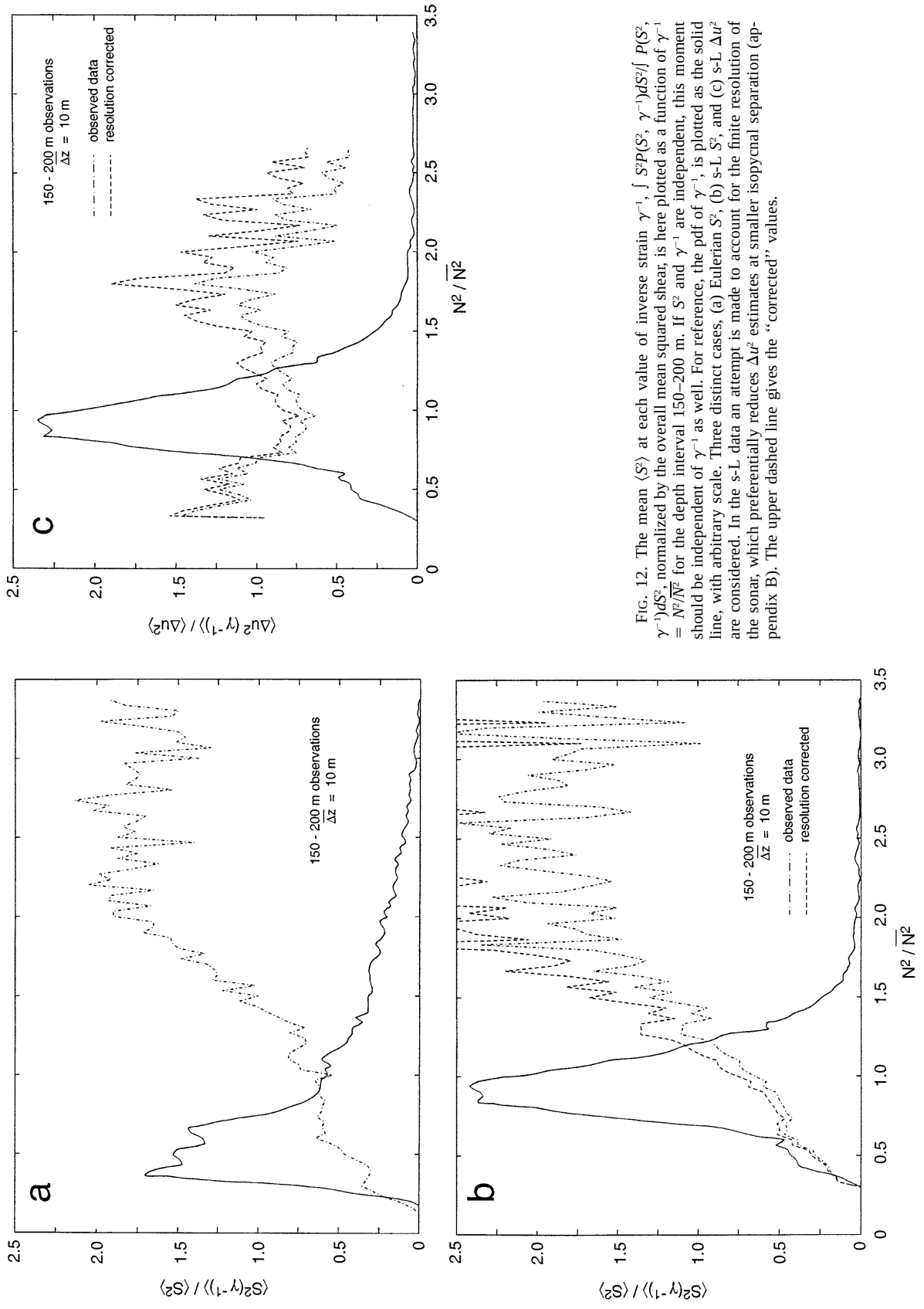

FIG. 12. The mean $\langle S^2 \rangle$ at each value of inverse strain γ^{-1}, $\int S^2 P(S^2, \gamma^{-1}) dS^2 / \int P(S^2, \gamma^{-1}) dS^2$, normalized by the overall mean squared shear, is here plotted as a function of $\gamma^{-1} = N^2/\overline{N^2}$ for the depth interval 150–200 m. If S^2 and γ^{-1} are independent, this moment should be independent of γ^{-1} as well. For reference, the pdf of γ^{-1}, is plotted as the solid line, with arbitrary scale. Three distinct cases, (a) Eulerian S^2, (b) s-L S^2, and (c) s-L Δu^2 are considered. In the s-L data an attempt is made to account for the finite resolution of the sonar, which preferentially reduces Δu^2 estimates at smaller isopycnal separation (appendix B). The upper dashed line gives the "corrected" values.

number of samples contributing to each estimate of $\langle S^2 \rangle$ or $\langle \Delta u^2 \rangle$. If these quantities are truly independent of γ^{-1}, the shear variance estimates should be horizontal lines. Even accounting for finite sonar resolution and noise (appendix B) there is significant variability in these curves.

In both the Eulerian and s-L frames, the expected value of S^2 increases monotonically with increasing γ^{-1}. The rapid increase in $\langle S^2 \rangle$ in the s-L frame (12b) is not the signature of measurement error. A fixed velocity precision corresponds to a shear noise variance that scales as γ^{-2}, rapidly increasing as isopycnal separation decreases. Such a noise can be modeled and subtracted from the observed $\langle S^2 \rangle$ estimates. Even when a sufficiently large noise is hypothesized that the residual signal becomes negative at large γ^{-1} ($\langle S^2 \rangle$ less than zero for $\gamma^{-1} > 3.5$, Fig. 12b), the basic increasing trend remains at smaller γ^{-1}.

In contrast to the s-L case, the influence of sonar noise is uniform as a function of strain in the Eulerian observations (Fig. 12a). The dramatic increase in $\langle S^2 \rangle$ for $\gamma^{-1} > \gamma^{-1}_{\text{mode}}$ is seen here as well.

The previous correlation study suggests that the s-L $\langle \Delta u^2 \rangle$ estimates might be independent of instantaneous strain. However, a more complicated picture appears in Fig. 12c, consistent with the visual interpretation of Fig. 10. The mean square velocity difference is largest for both uncommonly large ($\gamma^{-1} > 1.7$) and small ($\gamma^{-1} <$ .4) values of inverse strain. The apparent zero correlation between Δu^2 and N^2 is a consequence of the roughly symmetric variation of $\langle \Delta u^2 \rangle$ relative to the peak in the pdf of N^2.

The data support the proposition that neither S^2 nor Δu^2 is independent of N^2. Investigations at larger vertical separations support this general conclusion. The hypothesis that Δu^2 and N^2 are independent (H II) is a much better approximation than the corresponding assertion on S^2 and N^2 (H I). Significant departures from constancy in the $\langle \Delta u^2 \rangle$ versus N^2 curve occur at rarely experienced values of N^2. In contrast $\langle S^2 \rangle$ increases rapidly with N^2 for all but the largest values of N^2.

5. Discussion and summary

Observations of finescale shear, strain, and Richardson number have been obtained using Doppler sonar and profiling CTD systems mounted on the Research Platform *FLIP*. A significant qualitative observation is that the finescale shear field appears to be advected by the vertical displacement of both low- and high-frequency internal waves.

Statistical measures of the shear and Ri fields are formed in both Eulerian and isopycnal following frames. To a first approximation (neglecting strain), the pdfs of S^2 and Ri^{-1} are exponential. While there is some question as to whether turbulence in the sea is distributed lognormally, the inverse Richardson number certainly is not. This emphasizes the distinction between those processes that precede a mixing event and those that follow.

To model the Richardson number field more precisely the effects of strain must be included. It is also necessary to specify the statistical relationship between shear and strain. Two contrasting hypotheses are considered. The first holds that, in an s-L frame, cross-isopycnal variability in shear, $\Delta u(t)/\Delta z(t)$, is independent of isopycnal separation, $\Delta z(t)$. The alternative hypothesis maintains that cross-isopycnal velocity differences $\Delta u(t)$ are themselves independent of separation.

Using a Gamma probability density for the strain field (PA92), model pdfs of Ri are derived under both hypotheses. The inclusion of N^2, as well as S^2 fluctuations, is seen to result in the increased occurrence of extremely low and high values of Ri in the models. The data are adequate to confirm this general result.

The interesting physics here relates to the dependence/independence of shear and strain. Depending on the hypothesis selected, regions of low Ri are more likely to occur in layers of low (H I) or high (H II) Väisälä frequency. The observed pdfs of Ri are generally more consistent with H II, especially at the more commonly observed values of Ri. However, closer examination of the joint pdfs of shear and strain suggest that *neither* hypothesis is strictly correct.

The dependence of shear^2 fluctuations on strain is such that when N^2 is much less than its average value, S^2 is as well (Fig. 12a,b). Thus, the occurrence of low Ri events is reduced. This is consistent with Polzin's (1992) finding based on vertical profiling observations. We emphasize that, while low Ri events are less common than if N^2 and S^2 were independent, they are still more common than predicted by a model that neglects strain altogether (Figs. 9d–f).

The statistical dependence of shear and strain at small scales is not surprising. One can imagine two adjacent fluid layers defined by three isopycnal sheets. If two of the sheets converge locally (a low strain event), fluid must be exhausted laterally from the region. The resulting shear^2 depends on

$$\left| \frac{\partial^2}{\partial t \partial z} \gamma \right|.$$

Here S^2 and N^2 might be *uncorrelated*, given that only the absolute value of strain variation matters. However, they are not *independent.*

The two-dimensional nature of the SWAPP dataset has yet to be fully exploited. Specifically, the combined depth–time variability of Ri should be explored. The goal is to establish the appropriate timescale for low Ri events and to quantify the depth dependence of this scale.

Acknowledgments. The authors thank Eric Slater, Lloyd Green, Michael Goldin and Chris Neely for the design and construction of the CTD and sonar systems used in this effort, as well as their at-sea operation.

Discussions with Jerome Smith and Mark Merrifield proved extremely helpful. This work was supported by the Office of Naval Research under Contract N00014-94-1-0046 and the National Science Foundation Grant OCE91-10553. The support and cooperation of Bob Weller, Al Plueddemann, the other SWAPP investigators, and the crew of the Research Platform *FLIP* is appreciated.

APPENDIX A

Shear, Strain Covariance Modeling

Pinkel and Anderson (1992) have determined empirically that isopycnal separation statistics are well approximated by Gamma probability density functions. They consider the normalized isopycnal separation $\gamma \equiv \Delta z(t)/\overline{\Delta z}$ and consider the subset of the Gamma family (Erlang pdfs) constrained such that $\langle\gamma\rangle_{sL} = 1$, $\langle\gamma^{-1}\rangle_E = 1$:

$$P_L(\gamma|\overline{\Delta z}) = \kappa(\kappa\gamma)^{\kappa-1}\, e^{-\kappa\gamma}/\Gamma(\kappa) \qquad \text{(A1a)}$$

$$P_E(\gamma|\overline{\Delta z}) = (\kappa\gamma)^{\kappa}\, e^{\kappa\gamma}/\Gamma(\kappa). \qquad \text{(A1b)}$$

Here $\kappa = \kappa_0\overline{\Delta z}$, where κ_0 is a constant of the process. In the more familiar Gaussian framework κ_0^{-1} is the analog of the correlation scale of the strain field and κ_0 is the bandwidth of the vertical wavenumber spectrum of strain. In this non-Gaussian model, κ_0^{-1} also sets the magnitude of spectrum. All higher moments of the process are specified by κ_0, as well. Table A1 lists the first several moments of the process, as these are useful in the statistical modeling of strain, shear, Richardson number, and related quantities. It is important to note that this model is not supported by observations at scales smaller than approximately 3 m. In turn, many of the statistical quantities derived become singular at small κ.

Using the moments of the strain pdfs it is relatively easy to model a variety of statistical properties of interest. For example, using Eqs. (7) and (8), the expected values of Richardson number are

$$\langle \mathrm{Ri}^{-1}\rangle_{\mathrm{IL}} = \frac{\langle S^2\gamma\rangle_L}{\overline{N^2}} = \frac{\langle S^2\rangle_L}{\overline{N^2}} = \mathrm{Ri}_{\mathrm{IL}}^{*-1} \qquad \text{(A2a)}$$

$$\langle \mathrm{Ri}^{-1}\rangle_{\mathrm{IIL}} = \frac{\langle \Delta u^2\ \gamma^{-1}\rangle_L}{\overline{\Delta z^2}\ \overline{N^2}} = \frac{\langle \Delta u^2\rangle_L}{\overline{\Delta z^2}\ \overline{N^2}}\frac{\kappa}{\kappa-1} = \mathrm{Ri}_{\mathrm{IIL}}^{*-1}\frac{\kappa}{\kappa-1} \qquad \text{(A2b)}$$

$$\langle \mathrm{Ri}^{-1}\rangle_{\mathrm{IE}} = \frac{\langle S^2\gamma\rangle_E}{\overline{N^2}} = \frac{\langle S^2\rangle_E\langle\kappa+1\rangle}{\overline{N^2}} = \mathrm{Ri}_{\mathrm{IE}}^{*-1}\frac{\kappa+1}{\kappa} \qquad \text{(A2c)}$$

$$\langle \mathrm{R}^{-1}\rangle_{\mathrm{IIE}} = \frac{\langle \Delta u^2\gamma^{-1}\rangle_E}{\overline{\Delta z^2}\ \overline{N^2}} = \frac{\langle \Delta u^2\rangle_E}{\overline{\Delta z^2}\ \overline{N^2}} = \mathrm{Ri}_{\mathrm{IIE}}^{*-1}. \qquad \text{(A2d)}$$

In practice, it is difficult to make precise estimates of Ri at scales less than 10 m in the thermocline. Thus, $\kappa > 5$–10 for typical observations, and the differences between the various averages are slight.

TABLE A1. Moments of normalized strain.

$\kappa_0(\mathrm{m}^{-1})$	$\kappa = \kappa_0\overline{\Delta z}$ Semi-Lagrangian	$\gamma = \Delta z/\overline{\Delta z}$ Eulerian
$\langle\gamma^3\rangle$	$(\kappa+2)\cdot(\kappa+1)/\kappa^2$	$(\kappa+3)(\kappa+2)(\kappa+1)/\kappa^3$
$\langle\gamma^2\rangle$	$(\kappa+1)/\kappa$	$(\kappa+2)\cdot(\kappa+1)/\kappa^2$
$\langle\gamma\rangle$	1	$(\kappa+1)/\kappa$
$\langle\gamma^{-1}\rangle$	$\kappa/(\kappa-1)$	1
$\langle\gamma^{-2}\rangle$	$\kappa^2/(\kappa-1)(\kappa-2)$	$\kappa/(\kappa-1)$
$\langle\gamma^{-3}\rangle$	$\kappa^3/(\kappa-1)(\kappa-2)(\kappa-3)$	$\kappa^2/(\kappa-1)(\kappa-2)$

It is more instructive to examine covariances of specific interest. For example, if Δu^2 and γ are independent in an s-L frame (H II), then the covariance of S^2 and N^2 is given by Eq. (16). Using Table A1, this expression is easily evaluated, yielding

$$\begin{aligned}\langle S^2N^2\rangle_{\mathrm{IIL}} &- \langle S^2\rangle_L\langle N^2\rangle_L \\ &= \langle\Delta u^2\rangle_L\overline{N^2}/\overline{\Delta z^2}\ [\langle\gamma^{-3}\rangle - \langle\gamma^{-2}\rangle\langle\gamma^{-1}\rangle]_L \\ &= 2\kappa_o^2\langle\Delta u^2\rangle_L\overline{N^2}[\kappa/(\kappa-1)^2(\kappa-2)(\kappa-3)]. \qquad \text{(A3)}\end{aligned}$$

This is a positive covariance which, assuming $\langle\Delta u^2\rangle_L \sim \overline{\Delta z}^{+1}$, decreases with increasing mean separation.

In turn, if H I is in fact correct, one can evaluate the apparent covariance between Δu^2 and N^2 that must result:

$$\begin{aligned}\langle\Delta u^2N^2\rangle_L &- \langle\Delta u^2\rangle_L\langle N^2\rangle_L \\ &= \langle S^2\rangle_L\overline{N^2}\ \overline{\Delta z^2}\ [\langle\gamma\rangle - \langle\gamma^2\rangle\langle\gamma^{-1}\rangle]_L \\ &= -2\frac{\langle S^2\rangle_L\overline{N^2}}{\kappa_o^2}\left[\frac{\kappa^2}{\kappa-1}\right]. \qquad \text{(A4)}\end{aligned}$$

This covariance is negative. If $\langle S^2\rangle_L \sim \overline{\Delta z}^{-1}$, the covariance will have but weak dependence on $\overline{\Delta z}$.

Do large values of Ri^{-1} occur in sheets (regions of higher than average N^2) or in layers? Since $\mathrm{Ri}^{-1} \equiv S^2/N^2$, the covariance of Ri^{-1} and N^2 is just

$$\mathrm{cov}(\mathrm{Ri}^{-1},N^2) = \langle S^2\rangle - \langle\mathrm{Ri}^{-1}\rangle\langle N^2\rangle. \qquad \text{(A5)}$$

Considering averages formed in an s-L frame, the appropriate expression under H I is

$$\begin{aligned}\mathrm{cov}_{\mathrm{IL}}(\mathrm{Ri}^{-1},N^2) &= \langle S^2\rangle_L - \langle S^2\rangle_L\langle\gamma\rangle_L\langle\gamma^{-1}\rangle_L \\ &= -\langle S^2\rangle_L/(\kappa-1). \qquad \text{(A6)}\end{aligned}$$

The corresponding covariance formed in an Eulerian frame is just

$$\mathrm{cov}_{\mathrm{IE}}(\mathrm{Ri}^{-1},\ N^2) = -\langle S^2\rangle_E/\kappa.$$

Under H II the s-L covariance becomes

$$\begin{aligned}\mathrm{cov}_{\mathrm{IIL}}(\mathrm{Ri}^{-1},N^2) &= \frac{\langle\Delta u^2\rangle_L}{\overline{\Delta z^2}}[\langle\gamma^{-2}\rangle - \langle\gamma^{-1}\rangle^2]_L \\ &= \kappa_o^2\langle\Delta u^2\rangle_L/[(\kappa-1)^2(\kappa-2)]. \qquad \text{(A7)}\end{aligned}$$

The corresponding Eulerian II covariance is

$$\mathrm{cov}_{\mathrm{IIE}}(\mathrm{Ri}^{-1}\ N^2) = \kappa_0^2\langle\Delta u^2\rangle_E/[\kappa(\kappa-1)]. \qquad \text{(A8)}$$

Under H I, the s-L covariance is negative. Regions of low dynamics stability (large Ri^{-1}) are more likely to occur in regions of low static stability (s small N^2). Under H II the reverse is true! The conventional Eulerian H I covariance is negative, as is its s-L counterpart. The nonconventional Eulerian II covariance, based on observations from pairs of isopycnals that bracket a fixed reference depth, is also negative.

While this result emphasizes the fundamental importance of the shear-strain independence issue, several cautions are worthwhile. Specifically, it is possible that neither H I nor H II are valid. Also, as vertical scales decrease to the point where hydrodynamic instability is likely, the model strain pdfs are known to be in error.

APPENDIX B

Instrument Resolution and Noise

It has proven difficult to obtain reliable estimates of Richardson number variability on scales comparable to typical overturn scales in the thermocline (1–2 m). An objective of the present modeling effort is to infer the statistical behavior of Ri at small scales based on consistent application of principles determined from larger-scale observations.

This renders the issue of verifying the models problematic. The primary concern is with the velocity estimates, where both accuracy and resolution are an issue. The range resolution of a Doppler sonar is given by

$$\Delta z_{\text{res}} = 0.5c\langle T_p - \tau\rangle \cos\phi \qquad \text{(B1)}$$

(e.g., Pinkel and Smith 1992).

Here c is the speed of sound, T_p is the duration of the transmitted acoustic pulse, τ is the processing time lag, and ϕ is the angle of the sonar beam relative to vertical. For the 161-kHz system used in SWAPP, Δz_{res} equals 5.5 m (Anderson 1992). The finite resolution of the sonar reduced the variance of the observed velocity and shear estimates, presumably without affecting the Gaussianity of these signals.

In the attempt to develop velocity time series in isopycnal following coordinates, interesting problems can arise. As mentioned in section 5, if one asserts that H II is correct, velocity differences between isopycnal surfaces should be independent of the separation of these surfaces. However, as isopycnal pairs converge, approaching the resolution limit of the sonar, estimates of Δu^2 will be biased low. When the isopycnals diverge, the Δu^2 estimate will experience decreased bias. A spurious negative correlation between N^2 and Δu^2 results.

This effect can be modeled by assuming that the true correlation is zero, with γ^{-1} and Δu^2 statistically independent. If the true joint pdf is given by the separable product

$$P(\gamma^{-1},\Delta u^2|\overline{\Delta z}) = p_\gamma(\gamma^{-1}|\overline{\Delta z})\chi^2(\Delta u^2|\overline{\Delta z}), \qquad \text{(B2)}$$

we can create a resolution limited joint pdf by changing the variance of the χ^2 distribution as a function of γ^{-1}. In particular, as isopycnal separation is decreased, the variance of $\langle\Delta u^2\rangle$ in the χ^2 distribution can be decreased.

A recipe for implementing this variance decrease can be created, assuming that the true underlying shear spectrum is known. If, for example, the ''true shear spectrum'' is known, then it is easy to apply a model filter that mimics the resolution of the sonar, to produce a ''measured shear spectrum.'' From these ''true'' and ''measured'' spectra, ''true'' and ''measured'' velocity difference variances $\langle\Delta u^2\rangle(\overline{\Delta z})$ can be derived:

$$\langle\Delta u^2\rangle(\overline{\Delta z}) = \int S(k)\text{sinc}^2\left(\frac{k\overline{\Delta z}}{2\pi}\right) dk. \qquad \text{(B3)}$$

Here S(k) is the shear spectrum and sinc (x) $\equiv$ sin (πx)/(πx).

The finite resolution effect is modeled by choosing the Gargett et al. (1981) model shear spectrum as the true spectrum and a version multiplied by

$$\text{sinc}^2\left(\frac{k\cdot 5.5m}{2\pi}\right)$$

as the measured spectrum. The finite difference velocity variance of each is then calculated according to (B3). A set of χ^2 (exponential) pdfs is then generated,

$$\chi^2(\Delta u^2,\gamma^{-1}) = \frac{1}{\sigma(\gamma^{-1})}e^{-\Delta u^2/\sigma^2(\gamma^{-1})} \qquad \text{(B4)}$$

with variances adjusted according to the modeled variance ratio, assuming a mean isopycnal separation $\overline{\Delta z}$. The joint pdf (B2) is then generated, using Eq. (12) for p_γ. Since the first moment of Δu^2 is now a function of γ^{-1}, the pdf is no longer separable. This process can be repeated at a variety of $\overline{\Delta z}$, with the covariance of N^2 and Δu^2

$$\text{cov}(N^2,\Delta u^2) = \overline{N^2}\left[\int\int \gamma^{-1}\Delta u^2 P(\gamma^{-1},\Delta u^2|\overline{\Delta z})\, d\gamma^{-1}\, \Delta u^2 - \int\int \gamma^{-1}P(\gamma^{-1},\Delta u^2|\overline{\Delta z})\, d\gamma^{-1}\, \Delta u^2 \times \int\int \Delta u^2 P(\gamma^{-1},\Delta u^2|\overline{\Delta z})\, d\gamma^{-1}\, \Delta u^2\right] \qquad \text{(B5)}$$

calculated at each mean separation. The resulting apparent correlation due to finite sonar resolution is plotted in Fig. 11. The model variance reduction ratio $\langle\Delta u^2\rangle_{\text{measured}}/\langle\Delta u^2\rangle_{\text{true}}$ was used to ''correct'' the observed estimates of S^2 and Ri in Figs. 7b and 8b.

Noise in the sonar measurements is also a significant concern. SWAPP represents the first open ocean experiment where coded-pulse technology was used to improve sonar precision (Pinkel and Smith 1992). The 161-kHz sonar transmitted six repeats of a 7-bit Barker code. The duration of each bit was 0.25 ms, corresponding to

a nominal bandwidth of 4 kHz. The expected velocity precision of such a code is 0.74 cm s^{-1} after a one-minute (80 pulse) average.

In fact, the observed precision is considerably worse, more nearly 1 cm s^{-1} after six minutes of averaging. The major problem is not associated with the sonar, but rather the velocity field of the upper ocean. Surface wave velocities are two orders of magnitude more energetic than the low frequency motions of interest here. While wave motion decays rapidly with depth, the wave-induced motion of the sonar imparts a relative velocity, which is uniform with range. If the rms horizontal *FLIP* motion is of order 5 cm s^{-1} and associated primarily with the dominant swell at a 12-second period, then a six-minute (30 wave) average results in an rms velocity noise of order $5/\sqrt{30} = .9$ cm s^{-1}. With more advanced processing, one can attempt to remove this range-coherent noise on a pulse-by-pulse basis. However, this was not done in SWAPP.

The velocity imprecision has a significant effect on estimates of shear:

$$\langle \hat{S}^2 \rangle = \langle (u_1 + \epsilon_1 - u_2 + \epsilon_2)^2 \rangle / \overline{\Delta z}^2 = \langle (\Delta u)^2 \rangle / \overline{\Delta z}^2 + 2\langle \epsilon^2 \rangle / \overline{\Delta z}^2. \quad \text{(B6)}$$

As separation $\overline{\Delta z}$ decreases, the true velocity difference tends toward zero, leaving the noise to play a dominant role. Conversely the noise contribution decays as $\overline{\Delta z}^{-2}$ with increasing separation, whereas the signal tends to diminish as $\overline{\Delta z}^{-1}$. To model the effect of noise, a factor of $2\langle \epsilon^2 \rangle / \overline{\Delta z}^2$ was subtracted from the shear estimates in Figs. 7b and 8b, prior to the correction for sonar resolution.

Velocity imprecision can also influence covariance estimates of physical interest. For example, considering the covariance of S^2 and N^2 under H II, the role of noise can be easily seen:

$$\begin{aligned} &\mathrm{cov}(S^2, N^2) \\ &= \langle S^2 N^2 \rangle - \langle S^2 \rangle \langle N^2 \rangle \\ &= \frac{\overline{N^2}}{\overline{\Delta z}^2} [(\langle \Delta u^2 \rangle + 2\langle \epsilon^2 \rangle)(\langle \gamma^{-3} \rangle - \langle \gamma^{-2} \rangle \langle \gamma^{-1} \rangle)] \\ &= \frac{\overline{N^2}}{\overline{\Delta z}^2} \langle \Delta u^2 \rangle [(1 + NSR(\overline{\Delta z}))(\langle \gamma^{-3} \rangle - \langle \gamma^{-2} \rangle \langle \gamma^{-1} \rangle)]. \end{aligned} \quad \text{(B7)}$$

Here $NSR = 2\langle \epsilon^2 \rangle / \langle \Delta u^2 \rangle$ is the noise-to-signal ratio. Thus, while the noise contribution is significant, the role of the noise is easily modeled in these simple estimators.

REFERENCES

Anderson, S. A., 1992: Shear, strain, and thermocline vertical fine structure in the upper ocean. Ph.D. thesis, University of California, San Diego. [Available from University of California, San Diego, 9500 Gilman Dr., La Jolla, CA 92093.]

Bretherton, F., 1966: The propagation of groups of internal gravity waves in a shear flow. *Quart. J. Roy. Meteor. Soc.*, **92,** 466–480.

——, 1969: Waves and turbulence in stably stratified fluids. *Radio Sci.*, **4,** 1279–1287.

Briscoe, M. G., 1977: Gaussianity of internal waves. *J. Geophys. Res.*, **82,** 2117–2126.

Desaubies, Y. J. F., and M. C. Gregg, 1981: Reversible and irreversible finestructure. *J. Phys. Oceanogr.*, **11,** 541–556.

——, and W. K. Smith, 1982: Statistics of Richardson number and instability in oceanic internal waves. *J. Phys. Oceanogr.*, **12,** 1245–1259.

Eriksen, C. C., 1978: Measurements and models of fine structure, internal gravity waves, and wave breaking in the deep ocean. *J. Geophys. Res.*, **83,** 2989–3009.

Evans, D. L., 1982: Observations of small-scale shear and density structure in the ocean. *Deep-Sea Res.*, **29,** 581–595.

Gargett, A. E., P. J. Hendricks, T. B. Sanford, T. R. Osborn, and A. J. Williams III, 1981: A composite spectrum of vertical shear in the upper ocean. *J. Phys. Oceanogr.*, **11,** 1258–1271.

Garrett, C. J. R., and W. H. Munk, 1971: Internal wave spectra in the presence of fine structure. *J. Phys. Oceanogr.*, **1,** 196–202.

——, and ——, 1972: Ocean mixing by breaking internal waves. *Deep-Sea Res.*, **19,** 823–832.

——, and ——, 1975: Space-time scales of internal waves, A progress report. *J. Geophys. Res.*, **80,** 291–297.

Gregg, M. C., H. E. Seim, and D. B. Percival, 1993: Statistics of shear and turbulent dissipation profiles in random internal wavefields. *J. Phys. Oceanogr.*, **23,** 1787–1799.

Howard, L. N., 1961: Note on a paper of John W. Miles. *J. Fluid Mech.*, **10,** 509–512.

McKean, R. S., 1974: Interpretation of internal wave measurements in the presence of fine structure. *J. Phys. Oceanogr.*, **4,** 200–213.

Miles, J. W., 1961: On the stability of heterogeneous shear flows. *J. Fluid Mech.*, **10,** 496–508.

Munk, W. H., 1981: Internal waves and small scale processes. *Evolution of Physical Oceanography*, B. A. Warren and C. Wunsch, Eds., The MIT Press, 264–290.

Papoulis, A., 1984: *Probability, Random Variables, and Stochastic Processes.* 2d ed. McGraw-Hill, 576 pp.

Phillips, O. M., 1971: On spectra measured in an undulating layered medium. *J. Phys. Oceanogr.*, **1,** 1–6.

Pinkel, R., and S. Anderson, 1992: Toward a statistical description of finescale strain in the thermocline. *J. Phys. Oceanogr.*, **22,** 773–795.

——, and J. A. Smith, 1992: Repeat sequence codes for improved performance of Doppler sonar and sodar. *J. Atmos. Oceanic Technol.*, **9,** 149–163.

——, J. T. Sherman, J. A. Smith, and S. Anderson, 1991: Strain: Observations of the vertical gradient of isopycnal vertical displacement. *J. Phys. Oceanogr.*, **21,** 527–540.

Polzin, K. L., 1992: Observations of turbulence, internal waves, and background flows: An inquiry into the relationship between scales of motion. MIT/WHOI, WHOI-92-39, Woods Hole Oceanographic Institution, 243 pp.

Prudnikov, A. P., Y. A. Brychkov, and O. I. Marichev, 1986: Integrals and Series, I. (English Transl), Gordon and Breach, 798 pp.

Rubenstein, D., F. Newman, and R. Lambert, 1982: Coherence between stratification and shear in the upper ocean. Science Applications International Tech. Rep. SAI-82-614-WA, 20 pp. [Available from Science Applications International, P.O. Box 1303, McLean, VA 22102.]

Sherman, J. T., 1989: Observations of fine-scale vertical shear and strain in the upper-ocean. Ph.D. thesis, University of California, San Diego, 145 pp. [Available from University of California, San Diego, 9500 Gilman Dr., La Jolla, CA 92093.]